International Journal of Applied Engineering Research ISSN 0973-4562 Volume 13, Number 1 (2018) pp. 582-589

Design New control System for Brushless DC motor Using SVPWM

Farazdaq Rafeeq Yasien[1] and Roaa Abbas mahmood[1,2]

[1] *Department of Control and Systems Engineering, University of Technology, Baghdad, Iraq.*

[2]*Department of Renewable Energies, Ministry of Science and Technology, Baghdad, Iraq.*

Abstract

The conventional control system in a Brushless DC (BLDC) motor uses the Hall sensors for determining the position of the rotor that is needed for calculation of the back EMFs to generate the pulse width modulation (PWM) for three-phase inverter. However, these position sensors increase cost, size, noise signals and complexity in the control system. Therefore, this paper presents a new control system of the BLDC motor proposed through the elimination of the Hall sensors feedback signals and it depends on the motor speed feedback signal only. A new control system used the space vector modulation (SVPWM) technique to generate the PWM switching to three-phase inverter derive. PI controller has been used for the speed control of BLDC motor. Results obtained from comparison between the new control system (NCS) and conventional control system (CCS) of BLDC motor. The simulation tests for BLDC motor in a MATLAB/Simulink environment show that the NCS of BLDC motor is better than the CCS in tested in terms of transient response under different mechanical loads and speeds.

Keywords: BLDC motor, PWM, SVPWM, three phase inverter, and PI controller.

INTRODUCTION

The BLDC motors are rapidly gained popularity and become widely used in various consumer and industrial systems because of their better characteristics and performance. BLDC motor has several advantages over conventional DC motors and some of these are High efficiency, higher dynamic response, Better speed versus torque characteristics, Higher speed ranges, Long life operating, less noise operation, Less electromagnetic interference, Compact size, and better heat dissipation. BLDC motors are most commonly employed for robotics, computer peripherals, actuating drives, machine tools, electric propulsion and also for electrical power generation. With the development of sensorless technology besides digital control, these motors become so effective in terms of total system cost, size and reliability [1].

BLDC motor is type of permanent magnet synchronous motor (PMSM) which is driven by direct current and it accomplishes electronically controlled commutation system to produce rotational torque in the motor by changing phase currents depending on the rotor position.

Most BLDC motors have three Hall sensors for rotor position sensing where they either embedded into the stationary part of the motor or magnets on the rotor, but there are several drawbacks when such types of position sensors are used. The main drawbacks are the increased cost, size of the motor, and a special arrangement needs to be made for mounting the sensors. Further, Hall sensors are temperature sensitive and hence the operation of the motor is limited, which could reduce the system reliability because of the extra components and wiring [2].

Pulse width modulation (PWM) switching techniques are main part in the control system on the brushless DC motor drive. It's adjusted the three-phase bridge inverter to generate three-phase voltages controlling the BLDC motor. Many PWM switching techniques, , including the sinusoidal PWM (SPWM), carrier based PWM, selective harmonic elimination PWM, etc. are used for inverter controllers [3]. Space vector PWM (SVPWM) is one of the best methods because of its capability to minimize harmonic distortion. This approach is improved to achieve a high output voltage, minimize the harmonic output, and reduce the switching losses relative to other PWM techniques [4].

In the present study new control system of BLDC motor proposed through the elimination of the Hall sensors feedback signals and it depends on the speed motor feedback signal only.

A new control system used the SVPWM technique to generate the PWM switching to three-phase inverters derive. PI controller has been used for the speed control of BLDC motor.

CONTROL SYSTEM OF BLDC MOTOR DRIVE

The control system model of BLDC motor drive is designed through three main parts, which are BLDC motor, three-phase inverter and control system (PWM technique and speed controller) [5]. Figure 1 shows the block diagram configuration of control system scheme for BLDC motor.

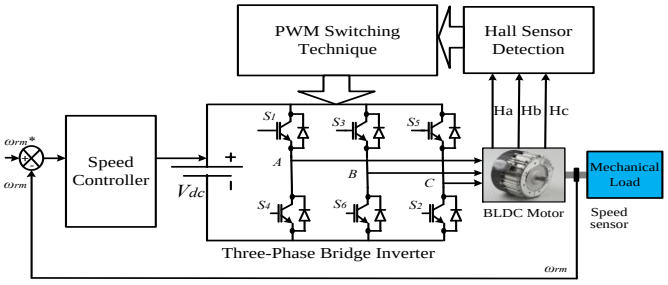

Figure 1: Block diagram of control system for BLDC motor drive.

TRADITIONAL CONTROL SYSTEM DESIGN PROCEDURE

Control system of BLDC motor required into main parts as shown in Figure 1. Control system required to four feedback signals, which are three hall sensor signals and speed motor signal.

The speed motor signal takes from speed sensor and it subtract from reference speed signal to generate the speed error signal.

Speed controller is received the error signal to generate the voltage source controller signal to three phase bridge inverter. Three-phase bridge inverter consists of six IGBTs switches as shown in Figure 1. Each switch has a freewheeling diode that protects the device from reverse voltage when the switch is turned off.

The six switches are divided into two groups; the positive group comprising upper switches S1, S3, and S5 and the negative group comprising switches S4, S6, and S2. Each phase has a pair of switches connected in parallel to the DC source. The controlled power flows to the load when the switches are tuned on and off. This tuning is created through the gates of the IGBTs, which are received from the PWM switching signals associated with the control system.

As for the Hall sensors feedback signals are produced the PWM waveforms through passing the Hall sensor detector and PWM switching techniques as shown in Figure 1. The Hall sensors are the most common sensor for predicting the rotor position of BLDC motor drive. The BLDC voltage vector is divided into six sectors, which is just a one-to-one correspondence with the Hall signal six states, as shown in Figure 2 [6].

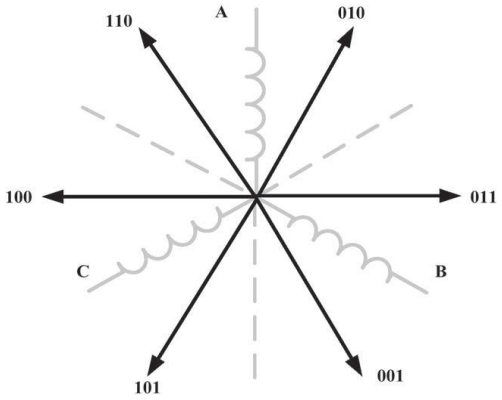

Figure 2: Six sectors of the BLDC motor voltage vector

Hall sensor detects rotor position to generate the controls switching of MOSFETs or IGBTs in three-phase bridge inverter drive for rotor position. Table (1) shows sequence for clock wise rotation when seen from shaft end. Hall sensor signals are 3-bit digit formed. A, B and C Hall sensors, while AH, BH, CH are upper switches drive and AL, BL, CL are lower switches drive. PWM is produced from the commutation sequence of hall sensor signal to control of three-phase inverter switches drive [7].

Table 1: Commutation sequence of Hall sensor signal

Rotor position (Degree)	Hall sensor signal	AH	BH	CH	AL	BL	CL
0-60	101	1	0	0	0	1	0
60-120	100	1	0	0	0	0	1
120-180	110	0	1	0	0	0	1
180-240	010	0	1	0	1	0	0
240-300	011	0	0	1	1	0	0
300-360	001	0	0	1	0	1	0

PI SPEED CONTROLLER

The closed loop speed control methods are traditionally implemented by conventional PI controllers. It is considered the most control technique that is widely used in control applications and it provides robust and reliable performance for most systems if the coefficients are tuned properly. Figure 3 shows the construction of a PI speed controller that receives an error speed signal from the BLDC motor. Thus, this controller generates an output signal that consists of the sum of errors and the integral of that error, as shown in the equation below:

$$u(t) = K_p\, e(t) + K_i \int_0^t e(t)\, dt \qquad (1)$$

where e is the error $e = (\omega_{refrence} - \omega_r)$, u is the control output signal, K_p is the proportional gain, and K_i is the integral gain. The performance of the PI speed controller mainly depends on the selected suitable PI parameters. Each parameter plays an important role in controlling the BLDC motor as shown in the Table 2 [8].

Table 2: Characteristics of PI control parameters

Type	Rise time	Overshoot	Settling time	Steady state error
K_p	Decrease	Increase	Small change	Decrease
K_i	Decrease	Increase	Increase	Eliminate

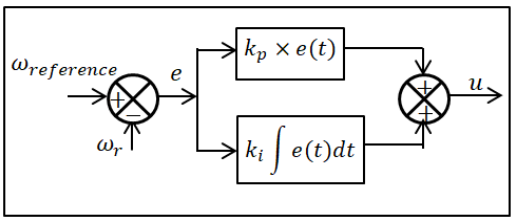

Figure 3: Construction of PI speed controller

NEW CONTROL SYSTEM DESIGN PROCEDURE

In this paper, new control system of BLDC motor proposed through the elimination of the Hall sensors feedback signals

and it depends on the speed motor feedback signal only as shown in Figure 4. A new control system is based on the space vector PWM technique to generate the PWM switching to three-phase inverter derives. The space vector PWM technique is received the speed motor signal converting to rotor angle to generate two voltages (V_α and V_β) as shown in Figure 5.

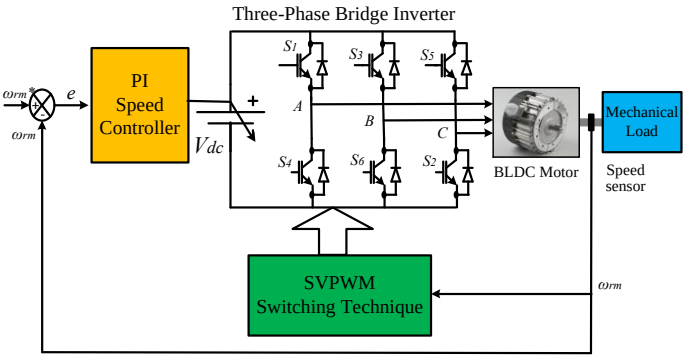

Figure 4: New control system of BLDC motor

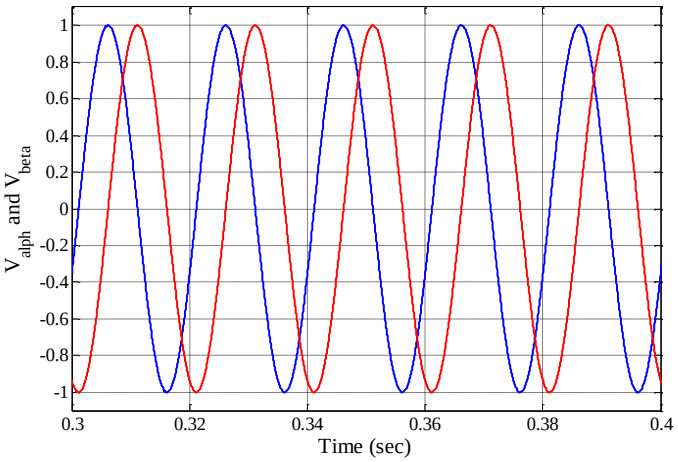

Figure 5: 5 cycles for V_α and V_β waveforms

Two-phase voltages (V_α and V_β) are used to obtain the magnitude of the reference voltage vector (V_{ref}) and the angle (α) between the voltage vectors using the Equation (2) and (3). Figure 6 shows the angle (α) for one cycle and also Figure 7 shows the number of sector.

$$|V_{ref}| = \sqrt{V_\alpha^2 + V_\beta^2} \quad (2)$$

$$\alpha = tan^{-1}\frac{V_\beta}{V_\alpha} \quad (3)$$

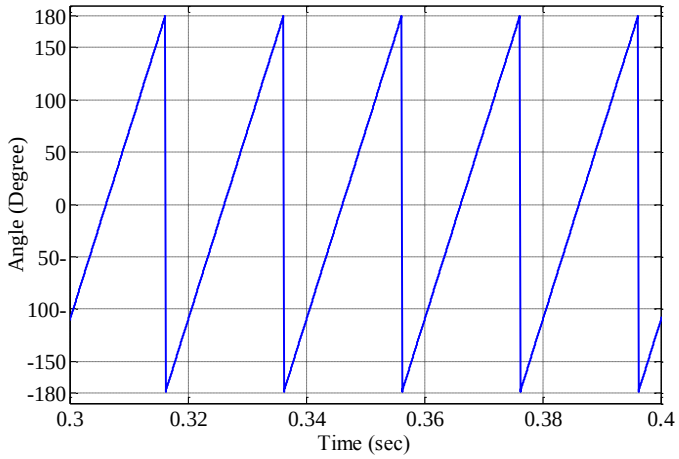

Figure 6: Waveform for 5 cycles for angle

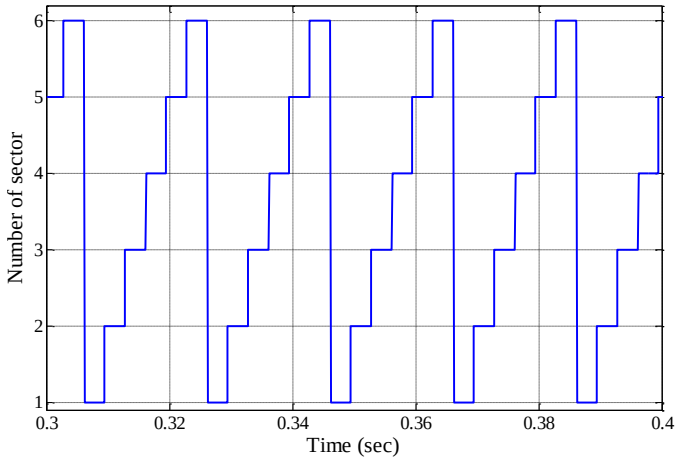

Figure 7: Waveform for 5 cycles for number of sector

Six sectors between the vectors is generated the hexagon frame as shown in Figure 8 [6].

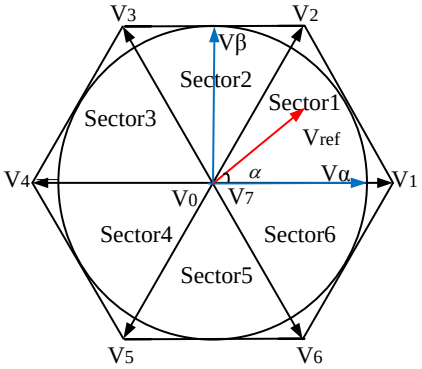

Figure 8: Hexagon diagram

SVPWM SWITCHING TECHNIQUE INVERTER

The SVPWM technique is used to generate the PWM control signals in the three-phase inverter. This approach is improved

to achieve a high output voltage, minimize the harmonic output, and reduce the switching losses relative to other PWM techniques. Moreover, the SVPWM technique is an advanced computation intensive PWM method and is possibly the best technique for VFD applications. Therefore, the SVPWM technique is one of the best methods because of its capability to minimize harmonic distortion.

As shown in Figure 9, the upper IGBTs (S1, S3, and S5 are equivalent to 1) are switched on, whereas the corresponding lower IGBTs (S2, S4 and S6 are equivalent to 0) are switched off. The on and off states of the upper IGBTs (i.e., S1, S3 and S5) can be used to determine the output voltage.

The relationship between the positive switching variable and the line-to-line voltages (V_{ab}, V_{bc}, V_{ca}) as well as the line-to-neutral voltages (V_{an}, V_{bn}, V_{cn}) can be expressed as follows [8].

$$\begin{bmatrix} V_{ab} \\ V_{bc} \\ V_{ca} \end{bmatrix} = V_{dc} \begin{bmatrix} 1 & -1 & 0 \\ 0 & 1 & -1 \\ -1 & 0 & 1 \end{bmatrix} \begin{bmatrix} S_1 \\ S_3 \\ S_5 \end{bmatrix} \quad (4)$$

$$\begin{bmatrix} V_{an} \\ V_{bn} \\ V_{cn} \end{bmatrix} = \frac{V_{dc}}{3} \begin{bmatrix} 2 & -1 & -1 \\ -1 & 2 & -1 \\ -1 & -1 & 2 \end{bmatrix} \begin{bmatrix} S_1 \\ S_3 \\ S_5 \end{bmatrix} \quad (5)$$

The six IGBTs in the inverter can form eight switch variables. Six of these switch variables are non-zero vectors (i.e., $V_1, V_2 \ldots\ldots, V_6$), and the rest are zero vectors (i.e., V_0, V_7) selected for the three upper IGBTs switches. The on and off patterns of the lower IGBTs switches are opposite to those of the upper switches. The voltage space vectors ($V_0, V_1, \ldots\ldots, V_7$) are determined Equations (4) and (5). The eight switching vectors, output line-to-neutral voltages, and output line-to-line voltages are shown in Figure 9 and Table 3.

The working principle of the SVPWM divides the output wave of the inverter into six sectors in a hexagon shape. Each sector lies between two voltage space vectors while the sector angle is 60 degree apart Figure (9) [9].

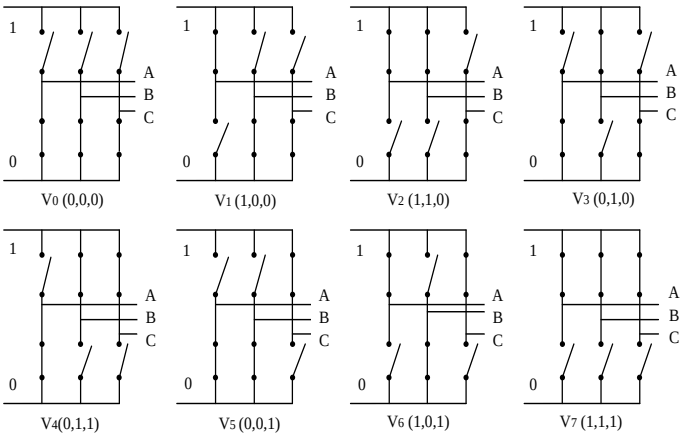

Figure 9: Eight states for the inverter voltage vectors (V_0 to V_7)

Table 3: Switching pattern of voltage space vectors

Voltage vectors	Switching vectors			Line to neutral voltage			Line to line voltage		
	S_1	S_3	S_5	V_{an}	V_{bn}	V_{cn}	V_{ab}	V_{bc}	V_{ca}
V_0	0	0	0	0	0	0	0	0	0
V_1	1	0	0	$2/3\,V_{dc}$	$-1/3\,V_{dc}$	$-1/3\,V_{dc}$	V_{dc}	0	$-V_{dc}$
V_2	1	1	0	$1/3\,V_{dc}$	$1/3\,V_{dc}$	$-2/3\,V_{dc}$	0	V_{dc}	$-V_{dc}$
V_3	0	1	0	$-1/3\,V_{dc}$	$2/3\,V_{dc}$	$-1/3\,V_{dc}$	$-V_{dc}$	V_{dc}	0
V_4	0	1	1	$-2/3\,V_{dc}$	$1/3\,V_{dc}$	$1/3\,V_{dc}$	$-V_{dc}$	0	V_{dc}
V_5	0	0	1	$-1/3\,V_{dc}$	$-1/3\,V_{dc}$	$2/3\,V_{dc}$	0	$-V_{dc}$	V_{dc}
V_6	1	0	1	$1/3\,V_{dc}$	$-2/3\,V_{dc}$	$1/3\,V_{dc}$	V_{dc}	$-V_{dc}$	0
V_7	1	1	1	0	0	0	0	0	0

The SVPWM technique receives a three-phase voltage (V_a, V_b, and V_c) separated by 120 degrees between two phases and converts it into two phases (V_α and V_β) with difference angle of 90 degrees using Clark's transformation Figure (8). The two-phase voltages (V_α and V_β) are used to obtain the magnitude of the reference voltage vector (V_{ref}) and the angle (α) between the voltage vectors in the hexagon. V_{ref} and α are located between the two adjacent non-zero vectors and the zero vectors, and they can be calculated as follows [9].

$$\begin{bmatrix} V_\alpha \\ V_\beta \end{bmatrix} = \frac{2}{3} \begin{bmatrix} 1 & -\frac{1}{2} & -\frac{1}{2} \\ 0 & \frac{\sqrt{3}}{2} & -\frac{\sqrt{3}}{2} \end{bmatrix} \begin{bmatrix} V_a \\ V_b \\ V_c \end{bmatrix} \quad (6)$$

V_{ref} is in sector 1, and can be synthesized by the vectors adjacent to it in that sector. Figure 10 shows the corresponding space vectors and time durations (T_1, T_2, and T_0) in sector 1. The time duration of V_{ref} is calculated through the product of the reference voltage and its sampling time period equal to the sum of the voltages multiplied by their time interval of space vectors in the chosen sector as shown in the following.

$$\int_0^{T_s} \bar{V}_{ref}\, dt = \int_0^{T_1} \bar{V}_1\, dt + \int_{T_1}^{T_1+T_2} \bar{V}_2\, dt + \int_{T_1+T_2}^{T_s} \bar{V}_0\, dt \quad (7)$$

$$T_s = T_1 + T_2 + T_0 \quad (8)$$

where T_s is the switching time calculated by $T_s = 1/f_s$

and f_s is the switching frequency. As shown in Equation (7), $\bar{V}_0$ applies a zero voltage to the output load. Consequently, the equation becomes:

$$T_s \bar{V}_{ref} = T_1 \bar{V}_1 + T_2 \bar{V}_2 \quad (9)$$

Substituting the values of $\bar{V}_1$ and $\bar{V}_2$ from Table (3) to the $\alpha\beta$ frame and analyse the voltage vectors yield the following:

$$T_s |V_{ref}| \begin{bmatrix} cos(\alpha) \\ sin(\alpha) \end{bmatrix} = T_1 \frac{2}{3} V_{dc} \begin{bmatrix} 1 \\ 0 \end{bmatrix} + T_2 \frac{2}{3} V_{dc} \begin{bmatrix} cos\frac{\pi}{3} \\ sin\frac{\pi}{3} \end{bmatrix} \quad (10)$$

$$T_1 = T_s \frac{3}{2} \frac{|V_{ref}|}{V_{dc}} \frac{sin\left(\frac{\pi}{3} - \alpha\right)}{sin\frac{\pi}{3}} \quad (11)$$

$$T_2 = T_s \frac{3}{2} \frac{|V_{ref}|}{V_{dc}} \frac{sin\alpha}{sin\frac{\pi}{3}} \quad (12)$$

The modulation index (MI) for the SVPWM is the relationship between the reference voltage magnitude and the DC voltage value shown in the following equation (Durgasukumar & Pathak 2012).

$$MI = \frac{|V_{ref}|}{\frac{2}{\pi} V_{dc}} \quad (13)$$

The time duration in the other sectors (n) can be calculated by substituting Equation (13) into Equations (11) and (12) and by using 60 degrees with α for each sector to become:

$$T_1 = \frac{\sqrt{3}.T_s.|V_{ref}|}{V_{dc}} sin\left(\frac{n}{3}\pi - \alpha\right) \quad (14)$$

$$T_2 = \frac{\sqrt{3}.T_s.|V_{ref}|}{V_{dc}} sin\left(\alpha - \frac{n-1}{3}\pi\right) \quad (15)$$

$$T_0 = T_s - (T_1 + T_2) \quad (16)$$

The four types of switching patterns are as follows: symmetric sequence, right aligned sequence, alternating zero vector sequence, and highest current not switched sequence [11]. All switching patterns must satisfy the following two conditions to minimize the device switching frequency. The change of the switching state from one to another involves only two switches in the same inverter leg. If either one of the switches is tuned on, then the other must be tuned off to reduce the switching frequency. The movement of V_{ref} from one sector to the next is achieved with the minimum number of switching to reduce the switching losses. Researchers have proven and recommended that the symmetric sequence method is the best method because it reduces the switching losses. Table 4 and Figure 10 show the presses for the symmetric sequence for each sector [7].

Table 4: Switching time calculation at each sector

Sector	Upper switching	Lower switching
1	$T_a = T_1 + T_2 + T_0/2$ $T_b = T_2 + T_0/2$ $T_c = T_0/2$	$\bar{T}_a = T_0/2$ $\bar{T}_b = T_1 + T_0/2$ $\bar{T}_c = T_1 + T_2 + T_0/2$
2	$T_a = T_1 + T_0/2$ $T_b = T_1 + T_2 + T_0/2$ $T_c = T_0/2$	$\bar{T}_a = T_2 + T_0/2$ $\bar{T}_b = T_0/2$ $\bar{T}_c = T_1 + T_2 + T_0/2$
3	$T_a = T_0/2$ $T_b = T_1 + T_2 + T_0/2$ $T_c = T_2 + T_0/2$	$\bar{T}_a = T_1 + T_2 + T_0/2$ $\bar{T}_b = T_0/2$ $\bar{T}_c = T_1 + T_0/2$
4	$T_a = T_0/2$ $T_b = T_1 + T_0/2$ $T_c = T_1 + T_2 + T_0/2$	$\bar{T}_a = T_1 + T_2 + T_0/2$ $\bar{T}_b = T_2 + T_0/2$ $\bar{T}_c = T_0/2$
5	$T_a = T_2 + T_0/2$ $T_b = T_0/2$ $T_c = T_1 + T_2 + T_0/2$	$\bar{T}_a = T_1 + T_0/2$ $\bar{T}_b = T_1 + T_2 + T_0/2$ $\bar{T}_c = T_0/2$
6	$T_a = T_1 + T_2 + T_0/2$ $T_b = T_0/2$ $T_c = T_1 + T_0/2$	$\bar{T}_a = T_0/2$ $\bar{T}_b = T_1 + T_2 + T_0/2$ $\bar{T}_c = T_2 + T_0/2$

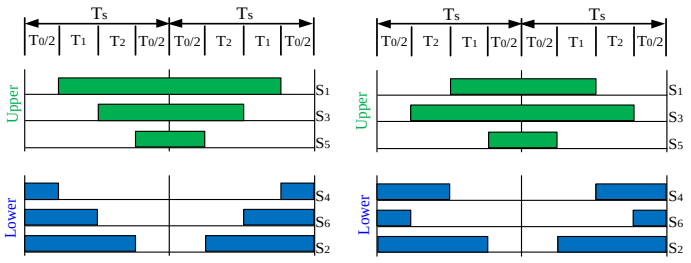

(a) (b)

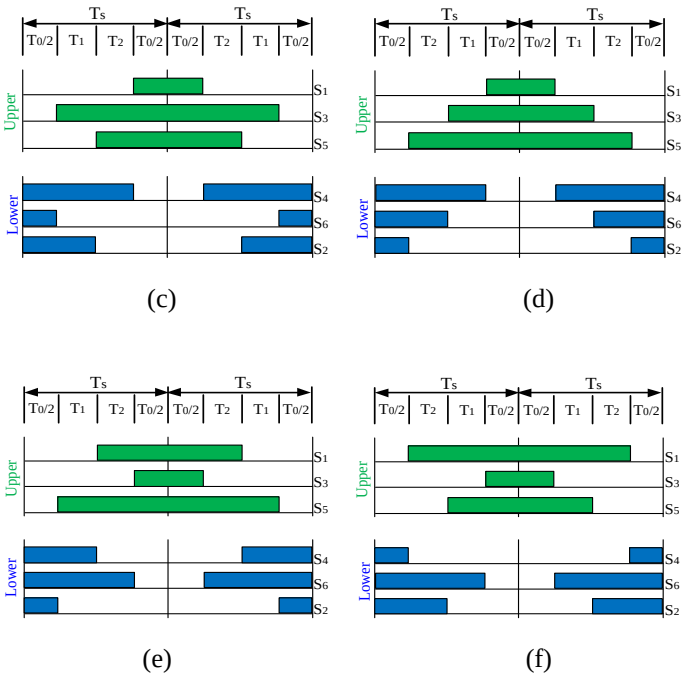

Figure 10: SVPWM switching patterns in (a) sector 1, (b)sector 2, (c) sector 3, (d) sector 4, (e) sector 5, and (f) sector 6

Figure 11 shows the SVPWM signal generation, inverter output voltages, and comparison of the three signals of the duty ratio waveform with the triangular waveform. This comparison is based on the condition $V_{DutyRatio} > V_{triangle}$, in which case $S = \text{ON}$; otherwise S = OFF,. In a bipolar switching scheme, each switch works opposite to the facing switch, similar to the case involving the comparison of the $V_{Ta\_DutyRatio}$ with the triangle waveform to generate the PWM signal for IGBT1 and the opposite IGBT4 in leg1, which is the same as leg2 and leg3 [9].

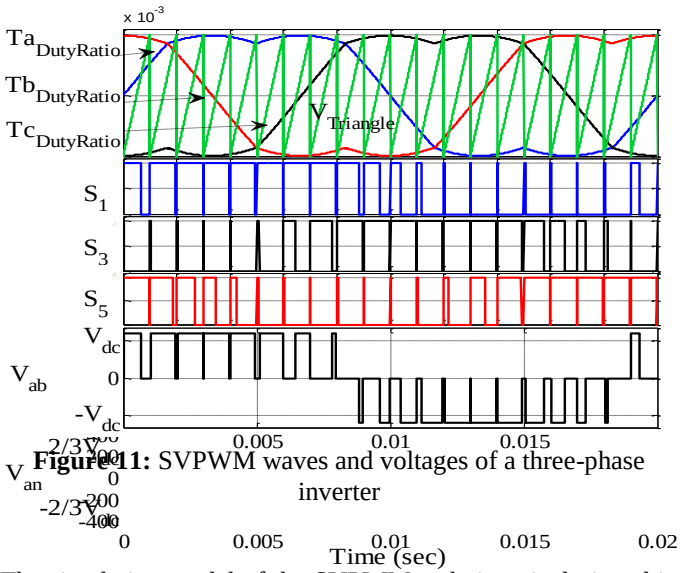

Figure 11: SVPWM waves and voltages of a three-phase inverter

The simulation model of the SVPWM technique is designed in MATLAB/Simulink in two steps. In the first step, the reference voltage (V_α), angle (α), and number of sectors are determined. Two voltages $(V_\alpha \text{ and } V_\beta)$ are received with this technique. The phase angle between the voltages is 90 degree. $V_\alpha \text{ and } V_\beta$ are transferred to the reference voltage (V_{ref}) and the angle (α) as shown in Equations (6). Figure (12) shows the simulation model of the first step. In the second step, the simulation model receives three signals (V_{ref}, α, n) and the DC voltage and switching time values are fixed. The times duration (T_1, T_2, T_0) are then calculated through the Equations (14), (15) and (16). Table (4) is used to determine the switching patterns in each sector. Figure (13) presents the simulation model of these calculations. In the final step of SVPWM simulation model, the switching signals to the IGBT devices are generated by comparing the duty ratio (T_a, T_b, T_c) with the up-triangle signal to generate the PWM for each IGBT device.

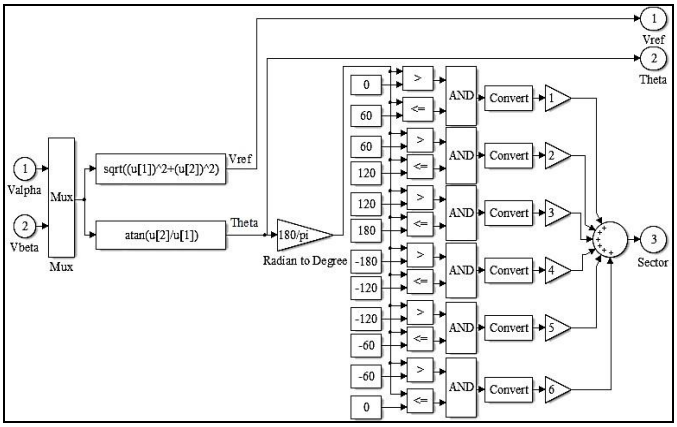

Figure 12: Simulation model of reference voltage, theta and number of sectors.

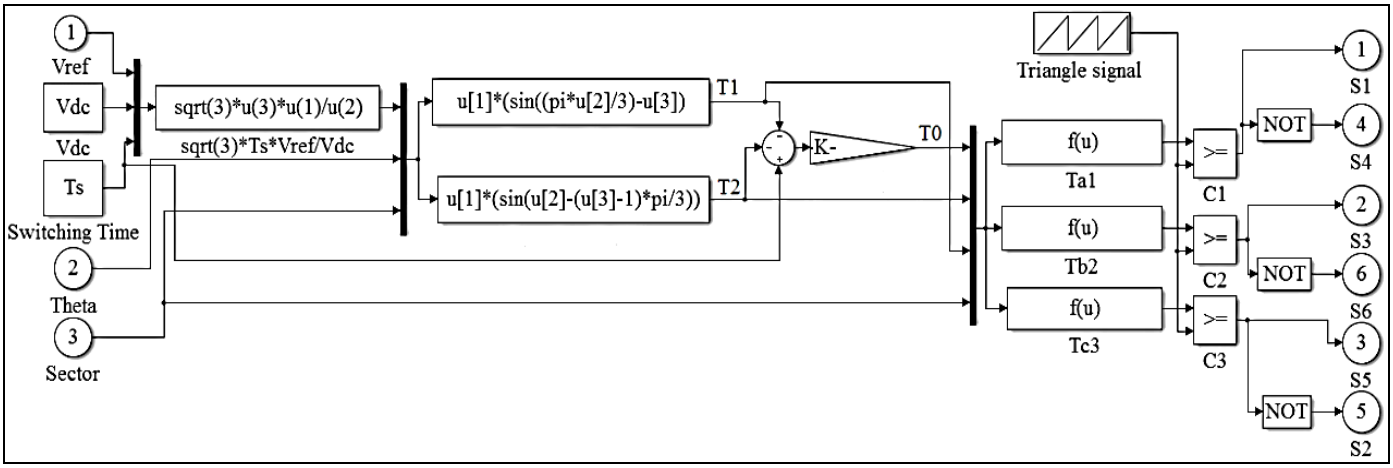

Figure 13: Simulation model of reference voltage, theta and number of sectors

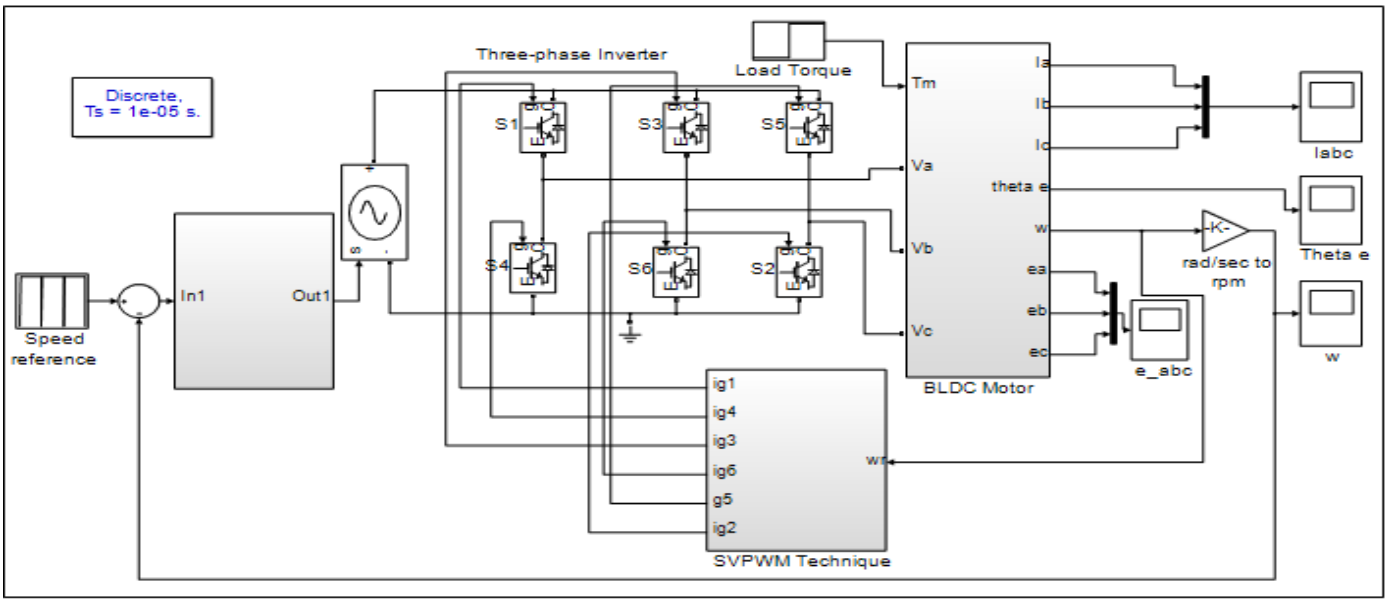

Figure 14: Simulation models of time duration and switching patterns

RESULTS

The simulation results are based on implementation and control schemes stated in the simulated model in Figure 14. The related results are used to validate the new control system of BLDC motor. In this work, the results are obtained from comparison between NCS and CCS, classical PI speed controller has been used for a control system of BLDC motor.

Figure 14 shows the speed response for NCS and CCS of BLDC motor. The NCS speed response is achived the best performance than CCS. Morover, the minimime of maximum overshoot, steady state error and setlling error. Figure 15 shows the three-phase curents for ramp response. This currents present 4.7 A from 0 to 0.5 sec because of the motor operated with no-load and increase the magnitude current until 10 A when the motor operated is full load. Figure 16 and Figure 17 show the three-phase voltages and EMFs at the same condition.

Figure 18 Electromagnetic Torque developed in N-m.

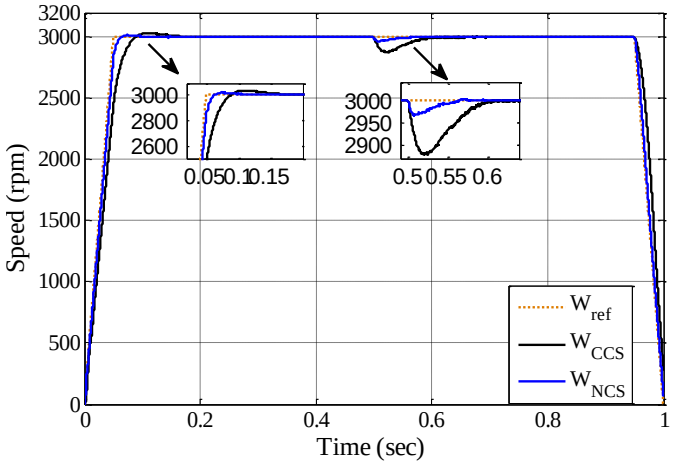

Figure 15: Speed response in rpm verses time.

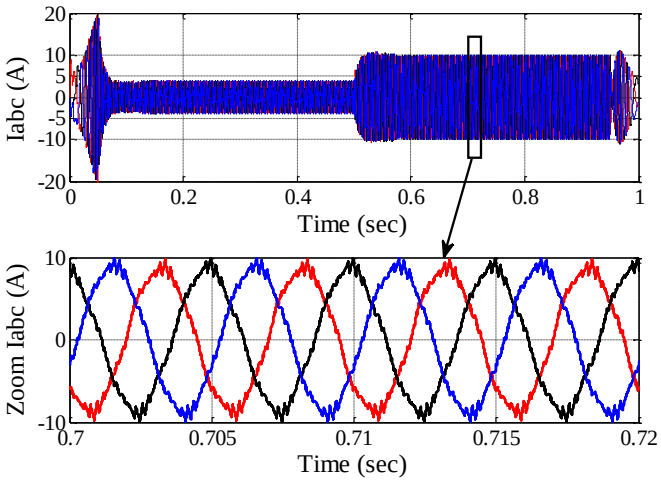

Figure 16: Three phase stator current

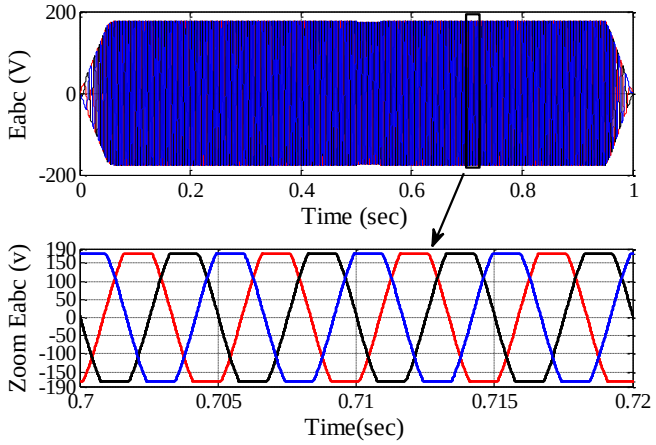

Figure 17: Three Phases back emf induced in the Stator

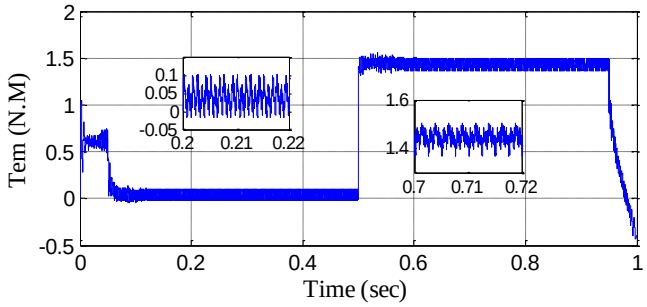

Figure 18: Electromagnetic Torque developed in N-m

CONCLUSIONS

New control system is proposed to improve the performance of BLDC motor through elimination from three Hall sensors for a less expensive, more reliable system, fast speed response of BLDC motor drive by SVPWM switching technique inverter.

PI controller has been used for the speed control of BLDC motor. The results has been obtained clearly displayed that the NCS speed response is better than the CCS speed response in terms of robustness, damping capability, and enhancement of transient responses of BLDC motor**.**

REFERENCES

[1] A. Niasar, A. Vahedi, and H. Moghbelli," Novel Position Sensorless Control of a Four-Switch, Brushless DC Motor Drive Without Phase Shifter" *IEEE Transactions on Power Electronics, Volume: 23, PP. 3079–3087, 2008.*

[2] J. Gamazo-Real, E. V zquez-Snchez, and J. Gmez-Gil, "Position and Speed Control of Brushless dc Motors Using Sensorless Techniques and Application Trends" *Sensors, volume. 10, NO. 7, PP. 6901-6947, 2010.*

[3] K. Kumar, P. Michael, J. John and S. Kumar, "Simulation and comparison of SPWM and SVPWM control for three phase inverter" ARPN Journal of Engineering and Applied Sciences, *volume* 5, NO. 7,PP. 61-74, 2010.

[4] Liang, W., Wang, J., Luk, P. C. K., Fang, W. & Fei, W, "Analytical modeling of current harmonic components in PMSM drive with voltage-source inverter by SVPWM technique" *IEEE Transactions on Energy Conversion, volume 29, PP. 673-680, 2014.*

[5] C. Xia, P. Guo, T. Shi and M. Wang,"Speed Control of Brushless DC Motor Using Genetic Algorithim Based Fuzzy Controller" *Proceedings of the 2004 International Conference on Intelligent Mechatronics and Automation Chengdu, PP. 460-464, 2004.*

[6] X. Nian, F. Peng, and H. Zhang," Regenerative Braking System of Electric Vehicle Driven by Brushless DC Motor" *IEEE Transactions on Industrial Electronics, volume 61 PP. 2798–2808, 2014.*

[7] Ameer L. Saleh and Adel A. Obed, "Speed Control of Brushless DC Motor based on Fractional Order PID Controller", *International Journal of Computer Applications Volume 95, No.4, PP. 0975 – 8887, 2014.*

[8] Mohammed A., and S. mahamood, "Control of Induction Motor Drive using Space Vector PWM", *International Conference on Electrical, Electronics, and Optimization Techniques (ICEEOT), PP. 3344-3351, 2016.*

[9] J.Sabarad and G.H. Kulkarni "Comparative Analysis of SVPWM and SPWM Techniques for Multilevel Inveter" *International Conference on Power and Advanced Control Engineering (ICPACE), PP. 232-237, 2015.*

[10] K. V. Kumar, P. A. Michael, J. P. John and S. S. Kumar "SIMULATION AND COMPARISON OF SPWM AND SVPWM CONTROL FOR THREE PHASE INVERTER", *ARPN Journal of Engineering and Applied Sciences, VOL. 5, NO. 7, PP. 61-74, 2010.*